Heliyon 9 (2023) e22108

Contents lists available at ScienceDirect

Heliyon

journal homepage: www.cell.com/heliyon

Photocatalytic effect of N–TiO_2 conjugated with folic acid against biofilm-forming resistant bacteria

Raphaella I.S. Oliveira [a,b], Iracema N. de Oliveira [b], Juliana F. de Conto [c], Augusto M. de Souza [d], Silvia R. Batistuzzo de Medeiros [d], Silvia M. Egues [c,e], Francine F. Padilha [a,f], Maria L. Hernández-Macedo [a,b,*]

[a] Graduate Program in Industrial Biotechnology, Tiradentes University, 49032-490, Aracaju, SE, Brazil
[b] Laboratory of Molecular Biology, Institute of Technology and Research, Tiradentes University, Aracaju, SE, Brazil
[c] Laboratory of Materials Synthesis and Chromatography, Center for Studies in Colloidal Systems, Institute of Technology and Research, Tiradentes University, Aracaju, SE, Brazil
[d] Department of Cell Biology and Genetics, Bioscience Center, Federal University of Rio Grande do Norte, 59078-900, Natal, RN, Brazil
[e] Graduate Program in Process Engineering, Tiradentes University, 49037-580 Aracaju, SE, Brazil
[f] Biomaterials Laboratory, Technology and Research Institute, Tiradentes University, Aracaju, Sergipe, Brazil

ARTICLE INFO

Keywords:
Resistant bacteria
Bacterial biofilm
Photocatalysis
TiO_2
Folic acid

ABSTRACT

Antibiotic resistance challenges the treatment of bacterial biofilm-related infections, but the use of nanoparticles as a treatment is a promising strategy to overcome bacterial infections. This study applied nitrogen-doped titanium dioxide (N–TiO_2) conjugated with folic acid (FA) on biofilm-forming resistant bacteria. The photocatalytic effect of TiO_2 nanoparticles (NPs) was studied under ultraviolet (UV), visible light, and dark conditions at 60, 120, and 180 min against planktonic cells and biofilms of *Staphylococcus aureus*, methicillin-resistant *Staphylococcus aureus* (MRSA), and *Pseudomonas aeruginosa.* TiO_2 NPs were in the anatase phase, spherical shaped with sizes of 10-13 nm, and effectively doped and conjugated with N and FA. The FA-conjugated nanoparticles (N–TiO_2-FA and FA-TiO_2) were shown to have a bactericidal effect on all bacteria between 60 and 180 min under UV and visible light conditions. Concerning biofilms, N–TiO_2-FA was shown to have a highly disruptive effect on all bacterial biofilms under UV irradiation at 180 min. Meanwhile, the nanoparticles did not show DNA damaging potential and they had no cytostatic effect, indicating that these NPs are biocompatible. In sum, nanoparticle conjugation with FA promoted photocatalytic effectiveness, revealing the promise this nanomaterial holds as a biocompatible antimicrobial agent.

1. Introduction

Biofilm formation determines virulence in many bacterial infections and lowers the susceptibility to antibiotics, meaning biofilm-forming bacteria challenge the treatment of persistent infections [1,2]. In that context, studies searching for solutions to reduce these pathogens' ability to form or disrupt biofilms are urgently needed, and the nanotechnology and nanoscience fields have become the focus of several biomedical studies, mostly regarding the applicability of photocatalytic nanoparticles such as titanium dioxide (TiO_2

* Corresponding author. nº 300 - Prédio do ITP (Universidade Tiradentes) - Farolândia, Aracaju, SE, 49032-490, Brazil.
E-mail address: lucyherma@gmail.com (M.L. Hernández-Macedo).

https://doi.org/10.1016/j.heliyon.2023.e22108
Received 17 March 2023; Received in revised form 8 September 2023; Accepted 4 November 2023
Available online 7 November 2023

NPs). Titanium dioxide is a metal oxide semiconductor widely studied due to its photocatalytic properties under UV radiation; it presents advantages such as low cost, low density, high specific strength, and great chemical stability [3,4]. These proprieties, especially in the TiO_2 anatase form, give it wide applicability, including as antimicrobial and anticancer agents [5–7].

The antimicrobial photocatalytic effect of TiO_2 is generated when reactive oxygen species (ROS) form under ultraviolet irradiation (UV), which excites an electron from the valence band to the conduction band, leaving a hole in the valence band of TiO_2, thus generating hydroxyl radicals and superoxide anions [8]. ROS exhibit significant oxidative potential that induces wall and cell membrane damage through lipid peroxidation, leading to cell death [8,9].

Many factors affect the performance of the photocatalyst in generating ROS, such as the wavelength of incident radiation, light intensity, chemical composition of the photocatalyst, physico-chemical properties, crystallographic phases, and surface functionalization, among others [3,4]. Currently, both the antimicrobial and the photocatalytic activities of TiO_2 can be improved by engineering hybrid nanosystems using metal conjugation (Ag, Cu), nonmetal doping (N, S), TiO_2-based heterojunctions, and phthalocyanine and folic acid conjugation [10–12].

TiO_2 activation requires a photon energy equal to or greater than its band gap ($h\nu \geq 3.20$ eV), which corresponds to wavelengths below 380 nm in the ultraviolet region [3,4]. The light absorption of TiO_2 must be modified in order to use this technology in indoor applications, such as self-cleaning surfaces and textiles or even human health treatments, since long-term exposure to UV irradiation has harmful effects on human cells. TiO_2 N-doping leads to a change in energy band structure to improve its visible light absorption, while maintaining the photocatalytic activity under ultraviolet light [13]. This improved photocatalytic activity of N-modified TiO_2 has been shown against Gram-negative and Gram-positive bacteria [14–16].

TiO_2 conjugation with folic acid has been suggested as a strategy to improve nanoparticle biocompatibility with target cells [17]. Folic acid (FA) is a vitamin of exogenous origin belonging to the B complex group; it is vital for prokaryotic and eukaryotic cells since it participates in the replication, repair, and methylation of DNA and regulates cell metabolic activities [18]. FA is composed of three regions: a central aromatic ring derived from *para*-aminobenzoic acid (PABA), a pteridine ring, and a chain of one or more glutamines. PABA is an essential compound that most bacteria, including *Escherichia coli*, need to produce FA [19]. While some bacteria can generate this and produce their own folic acid through metabolic biosynthetic enzymes [20], others do not have this characteristic and, therefore, require FA from the external environment for their cell replication [21].

In the literature, some works are reported in which nanoparticles were coated with FA to increase their biocompatibility and improve their performance as antibacterial agents through the delivery of drugs against bacteria. Chowdhuri et al. (2015) [22] developed silver nanoparticles conjugated with folic acid to increase antibacterial activity and reported a decrease in bacterial growth and viability values in Gram-negative (*E. coli*) and Gram-positive (St*aphylococcus aureus*) bacteria. Chen et al. (2018) [17] synthesized a multilayer nanocarrier using mesoporous silica covered with a bilayer of folic acid and calcium phosphate. The material showed a strong capacity to target bacterial infections in vivo, and this capacity was enhanced by the FA property. The researchers also loaded the nanoparticles with the antibiotic ampicillin and observed an increased uptake and reduced efflux effect in *E. coli* and *S. aureus* through the specific targeting of FA. Semiconductor nanoparticles such as ZnO were also conjugated with FA to obtain greater biological activity in bacterial folate receptors through the coupling [23]. El-Borady and El-Sayed (2020) [23] examined the antimicrobial efficacy of ZnO-FA against *E. faecalis* and *E. ludwigii* and verified the nanoparticle anchorage at several sites of the cell, causing damage to the membrane, which ended in lyse cells. Similar works with ZnO-FA nanoparticles also showed better antibacterial activity than the pure compounds against *S. aureus* [24–27]. All works attribute the antibacterial action of ZnO nanoparticles to the generation of ROS, which can lead to lipid peroxidation and oxidative stress of the cell, and consequently, membrane rupture and DNA damage [23]. However, none of these materials have been studied in bacterial biofilm disruption.

It seems that, given the importance of FA for cellular metabolism, it can be strategically used to conjugate TiO_2 nanoparticles coated with other compounds. Nanoparticles formed of Cd–TiO_2/PEG/FA and AgCl/TiO_2/FA, for example, were used as antimicrobial material or in the development of antimicrobial material against *E. coli* and S. *aureus* [28–30]. With regard to biofilms, the conjugation of TiO_2 alone has not yet been reported as an antibiofilm agent, despite the construction of TiO_2 nanoparticles coated with other compounds, which have been reported as disruptors of *E. coli* and *S. aureus* biofilms [31–33]. In these studies, UV light was not used to activate TiO_2 in the photocatalytic reaction to obtain greater antibiofilm or antibacterial activity. The literature shows that the study of nanoparticles of TiO_2 conjugated to folic acid is still little explored as an antimicrobial agent, though it seems to hold potential mainly for the disruption of bacterial biofilms, which are protective barriers challenging treatment with antibiotics [1].

In that context, this work contributes to developing a new alternative approach of using folic acid conjugation of N–TiO_2, without any chemical ligand, against planktonic cells and biofilm-forming resistant bacteria. N-doped TiO_2 conjugated with FA (N–TiO_2-FA) and TiO_2 conjugated with FA (TiO_2-FA) were synthesized and characterized, and their antibacterial and antibiofilm properties were assessed against *Staphylococcus aureus*, methicillin-resistant *Staphylococcus aureus* (MRSA), and *Pseudomonas aeruginosa*.

2. Materials and methods

2.1. Chemicals

The chemicals and materials used for the synthesis were titanium tetraisopropoxide [Ti $(OC_3H_7)_4$, 99.5 %, Sigma–Aldrich] and ethylmethylamine (C_3H_9N, 99.0 %, Sigma- Aldrich). The TiO_2 used as a reference in this study was Aeroxide TiO_2 P25. The FA (≥97 %) tablets were purchased from a local drugstore and ground before use.

2.2. Synthesis of TiO_2 and nitrogen-doped TiO_2 nanoparticles

The TiO_2 synthesis was performed according to Ref. [34] with modification. A solution containing 30 mL of ethyl alcohol and 20 mL of titanium tetraisopropoxide ($Ti[OCH(CH_3)_2]_4$) was prepared under magnetic stirring. After homogenization, 100 mL of distilled water was added, and the sample was separated by decantation at room temperature for 48 h. The solid residue was dried, macerated, and submitted to calcination at 105 °C for 30 min, with a heating rate of 5 °C/min, followed by heating at 400 °C for 120 min using a muffle (Q318M24 Quimis).

For the N-doped TiO_2 synthesis, the methodology described by Ref. [35] was used with modification. Briefly, two solutions were prepared under magnetic stirring: Solution 1 (5.0 mL triethylamine and 95 mL deionized water at pH 2), and Solution 2 (20 mL titanium tetraisopropoxide and 30 mL ethyl alcohol). Both solutions were mixed, adjusted to pH 7, and stirred for 1 h. Then, the material was decanted, washed, dried, and calcined at 400 °C as described before.

2.3. Folic-acid-conjugated TiO_2

The conjugation of TiO_2 with folic acid was performed according to the procedure in Ref. [36] with some modification, using a FA/TiO_2 ratio of 20 %. A 0.1 M sodium bicarbonate ($NaHCO_3$) solution was prepared with 0.02 g of folic acid and adjusted to pH 5.5 with HCl. The TiO_2 and N–TiO_2 NPs (0.1 g/mL) previously synthesized were dispersed in deionized water by sonication for 10 min, added slowly to the FA solution, and stirred for 24 h in the dark. The nanoparticles were collected using a centrifuge at 8000×*g* for 15 min and subjected to washing in deionized water, followed by ethanol, and then dried overnight at 50 °C.

2.4. Characterization of TiO_2 nanoparticles

The UV–Vis diffuse reflectance spectra (UV-DRS) of the TiO_2, N–TiO_2, FA-TiO_2, and N–TiO_2-FA samples were measured using a Shimadzu spectrophotometer, model UV-2600, in the range from 200 nm to 800 nm. The structural properties of the synthesized TiO_2 NPs and TiO_2 P25 used as reference were evaluated with X-ray diffraction (XRD) using a Panalytical EMPYREAN diffractometer equipped with a CuKα source ($\lambda = 1.54178$ Å). The functionalization and conjugation of TiO_2 NPs with FA and nitrogen were analyzed by attenuated total reflectance Fourier-transform infrared spectroscopy (ATR-FTIR) in the range of 4000–800 cm^{-1} and with a 2 cm^{-1} resolution, using the Cary 630 FTIR spectrometer (Agilent Technologies, USA). The morphology of TiO_2 NPs was analyzed with transmission electron microscopy (TEM) using MET JEOL JEM 1011 equipment at 60 kV. Before taking the TEM measurements, the samples (in 1000 ppm) were sonicated at 50 Hz for 10 min at intervals of 2 min, and then drops of the suspension were placed on carbon-coated copper grids and dried for analysis.

2.5. Bacterial strain

Planktonic (free-living) bacteria and biofilms of *Staphylococcus aureus* ATCC 25923 INCQS 00015, MRSA ATCC 43300 INCQS 00577, and *Pseudomonas aeruginosa* ATCC 27853 INCQS 00099 were used for the photocatalytic tests. These strains were provided by the National Institute for Quality Control in Health (INCQS) of the Oswaldo Cruz Foundation (FIOCRUZ) and grown on brain–heart infusion broth (BHI) and/or Mueller–Hinton agar (MHA) for 24 h at 37 °C, before biofilm production and photocatalytic assays.

2.6. Bacterial biofilm production

The biofilm formation was evaluated with a procedure described in Ref. [37], using 1.5×10^8 CFU/mL of *S. aureus,* MRSA, and *P. aeruginosa* added to a 96-well flat-bottomed polystyrene plate containing BHI. After 24 h at 37 °C, the medium was discarded. Next, we added 2 % violet crystal (w/v), washed with sterile water, and added 95 % ethanol for analysis in a microplate reader (Biochrom EZ Read 2000) at 595 nm. The strains *Staphylococcus epidermidis* ATCC 35984 (biofilm producer) and *Staphylococcus epidermidis* ATCC 12228 (non-biofilm producer) were used as positive and negative controls, respectively. The classification of bacterial biofilm was evaluated according to the method established by Ref. [38].

2.7. Antibacterial and antibiofilm activity analysis

The antimicrobial activity of NPs on planktonic bacteria was evaluated using photocatalytic assays according to the adapted minimum inhibitory concentration (MIC) method [39]. Briefly, 1 mg/mL of previously sonicated TiO_2 NPs was added to a bacterial suspension with 1.5×10^8 CFU/mL in saline solution (0.9 % NaCl), and it was exposed to visible light, UV light, and dark conditions. A fluorescent lamp (Philips 8W T5, $\lambda > 400$ nm) at ~ 0.5 mW cm^{-2} and UV lamp (Philips 8W BLB T5, $\lambda = 365$ nm) were used in the visible light and UV light tests, respectively. After photocatalysis at 0, 60, 120, and 180 min, 10 μL aliquots of the bacterial suspension were inoculated in sterile 96-well polystyrene microplates containing BHI 2X broth, and those were incubated at 37 °C for 24 h. The bacterial viability was evaluated at 595 nm using 20 μL of 0.5 % (w/v) 2,3,5 triphenyl tetrazolium chloride (TTC) at 37 °C for 2 h. Samples were analyzed in triplicate and assays without a photocatalyst were used as a control under visible light, UV light, and dark conditions.

Antibiofilm activity was studied using TiO_2 NPs (1 mg/mL) in BHI previously dispersed in ultrasound for 1 h. Nanoparticles were added to the biofilm prepared on glass coverslips. Those were added to a 96-well polystyrene microplate (item 2.6), and it was exposed

to visible light, UV light, and dark conditions for 180 min. Then, the samples were stained with violet crystal (2 % v/v) for 5 min, and color excess was removed using deionized water. We added 95 % ethanol to the stained biofilm, and that was agitated for 5 min. Then, the material was measured at 595 nm using an ELISA reader. Biofilms on the glass coverslips were analyzed with atomic force microscopy (AFM; SPM-9700 Shimadzu, Kyoto, Japan), using the dynamic mode at 300 kHz and 40 N m^{-1}. The analyses were performed at five random points on each coverslip with a 20 × 20 μm scale. The images were processed using the equipment's software (SPM-9700 Shimadzu).

2.8. Cell viability in MTT assay

An MTT assay was performed according to the procedure in Ref. [40] with minor modifications. Chinese hamster ovary cells (CHO–K1) (1×10^4 cells/well) were seeded in a 96-well plate containing 100 μL/well of Dulbecco's modified Eagle's medium (DMEM) and phenol red supplemented with 1 % streptomycin, 1 % glutamine, and 10 % fetal bovine serum (FBS). After 24 h of incubation (37 °C, 5 % CO_2, 90 % humidity), the cells were exposed to the TiO_2 NPs at 1 mg/mL, 0.5 mg/mL, and 0.25 mg/mL for 24 h. Then, cells were washed twice with a fresh cell culture medium and incubated with 1 mg/mL MTT (3–4, 5 dimethylthiazol-2, 5 diphenyl tetrazolium bromide) in phosphate-buffered saline (PBS) at 37 °C for 4 h. The medium was removed and then 200 μL of 100 % DMSO (dimethyl sulfoxide) was added to trigger the solubilization of purple formazan crystals, following which we measured the absorbance at 570 nm. Medium without photocatalysts (untreated) was used as a negative control, and medium with 1 % SDS was used as a positive control. The results were normalized to the untreated control and expressed as % viability.

2.9. Cytokinesis-block micronucleus assay (CBMN)

To test the genotoxic potential of TiO_2 NPs, we performed a CBMN assay according to the procedure in Ref. [41] with minor modifications. Briefly, CHO–K1 cells (2×10^4 cells/well) were plated in 24-well plates containing 500 μL/well DMEM supplemented with 1 % streptomycin, 1 % L-glutamine, and 10 % FBS. Cells were maintained at 37 °C, 5 % CO_2, and 90 % humidity for 24 h. Then, cells were exposed to TiO_2 NPs at 1 mg/mL, 0.5 mg/mL, and 0.25 mg/mL. After 24 h, the cells were washed with PBS and re-incubated in fresh media containing 5 μg/mL cytochalasin-B (Sigma–Aldrich, Saint Louis, MO, USA). Untreated cells and CHO–K1 cells exposed to 0.5 μM mitomycin were used as negative and positive controls, respectively. After incubation (for 24 h), cells were trypsinized using 200 μL of 0.025 % trypsin for 5 min and neutralized with 600 μL of basal culture medium. The cell suspensions were centrifuged (2500×*g*/8 min), and the cells were fixed three times with a freshly prepared glacial acetic acid:methanol solution (9:1, v/v). Next, 60 μL of the fixed cells was placed on glass slides, air dried at 60 °C, and stained with a 5 % (v/v) Giemsa solution. Frequencies of micronuclei (MNs), nucleoplasmic bridges (NPBs), and nuclear buds (NBUDs) in the cells submitted to nanoparticles were analyzed. The nuclear division index (NDI) was calculated using the following formula: [NDI = M1 + 2(M2) + 3(M3) + 4(M4)/N], where M1–M4 represents the number of cells with 1–4 nuclei, respectively, and N is the total number of scored cells.

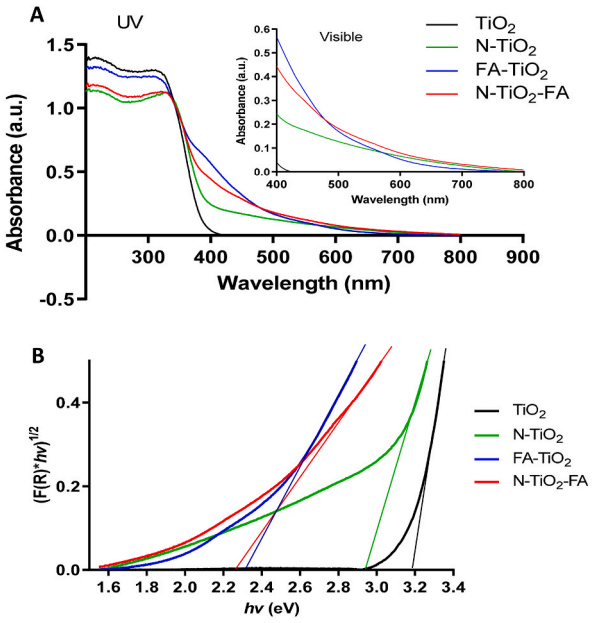

Fig. 1. (**A**) Diffuse reflectance spectrum UV–Vis of TiO_2, N–TiO_2, FA-TiO_2 and N–TiO_2-FA. The inserted figure shows the widening of the spectrum in the visible region. (**B**) *Band gap* energy of TiO_2 (3.19 eV), N–TiO_2 (2.94 eV), FA-TiO_2 (2.32 eV) and N–TiO_2-FA (2.26 eV) samples.

2.10. Statistical analysis

Triplicate analyses of microbial growth, biofilm production, and photocatalysis were performed using GraphPad Prism 5 (GraphPad Software Inc., San Diego, USA). Statistical values were expressed as mean ± standard deviation (SD) and calculated using one-way analysis of variance (ANOVA) with Tukey's post hoc comparison. Values of $p < 0.05$ were considered significant.

3. Results and discussion

3.1. Characterization of the TiO_2 nanoparticles

UV-DRS was used to investigate the optical proprieties of TiO_2, N–TiO_2, FA-TiO_2, and N–TiO_2-FA nanoparticles [Fig. 1]. A high absorption region between 200 and 350 nm was observed in pure TiO_2 samples, as well as in nanoparticles with FA and those that were N-doped [Fig. 1 (A)]. In the visible region ($\lambda > 400$ nm), FA-TiO_2 and N–TiO_2- FA exhibited greater absorption than N–TiO_2, evidencing the capacity for photon absorption under visible light of nanoparticles conjugated to FA. These photocatalysts with FA also exhibited a decrease in band gap energy [Fig. 1 (B)], confirming their ability to absorb in the visible light spectrum. The absorption in visible light may be due to the chromophore characteristics of FA, which support absorption in the UV region and can extend that to the visible region [42].

The crystalline structure of the synthesized nanoparticles was analyzed with XRD [Fig. 2]. Characteristic peaks for TiO_2 at $2\theta =$ 25.2°, 37.8°, 48.2°, 54.1°, 55.0°, 62.7°, 69.0°, 70.4°, and 75.0° were observed, which were assigned to the lattice planes (101), (004), (200), (105), (211), (204), (116), (220), and (215), attributed to the anatase phase [43]. The crystal structure of commercial TiO_2 P25 was also evaluated, and the diffractogram showed characteristic peaks of both anatase and rutile with lattice planes (110) and (101), respectively [44]. Conversely, reflections corresponding only to the anatase form in the nanoparticles synthesized in this work were observed. This result was consistent with the calcination temperature used in the synthesis process (<500 °C), as the anatase–rutile phase transition occurs at higher temperatures [45].

To verify the N-doping and FA conjugation in the photocatalysts, FTIR analyses were performed [Fig. 3]. All TiO_2 samples exhibited a peak at around 1630 cm^{-1}, assigned to the stretching vibration of O–H groups from the adsorbed water on the TiO_2 surface [Fig. 3 (A)]. The TiO_2 N-doping was evidenced by a peak at 1400 cm^{-1}, which changes during FA conjugation [36,46].

In addition, peaks at around 1696 cm^{-1}, 1607 cm^{-1}, and 1485 cm^{-1} were observed in FA, FA-TiO_2, and N–TiO_2-FA samples [Fig. 3 (A)]. These peaks correspond to the carbonyl C═O, N–H, and pteridine ring vibrations, respectively [47]. The pteridine ring is a component of folic acid, and the peak at 1485 cm^{-1} in these samples suggests the conjugation of FA to TiO_2.

The peaks at around 1512 cm^{-1} and 1440 cm^{-1} observed in samples with FA correspond to carboxylate salt and suggest bonding between the carboxylic acid of FA and the titanium atom [36]. Absorption peaks from 3500 to 3000 cm^{-1} in TiO_2 and N–TiO_2 samples were attributed to hydroxyl groups [46] [Fig. 3 (B)]. The samples conjugated to folic acid (FA-TiO_2 and N–TiO_2-FA) showed lower intensity of this band, suggesting that FA interacts with the hydroxyl groups of TiO_2.

The FA spectra showed an absorption band at around the 3555 cm^{-1} and 3416 cm^{-1} regions [Fig. 3 (B)]. According to Ref. [48], this band is attributed to the axial stretching of O–H and N–H bonds in the pteridine ring. These characteristic peaks of FA with modification were observed in FA-TiO_2 and N–TiO_2-FA samples, indicating the FA conjugation to TiO_2.

The morphology and size of the nanoparticles were characterized with TEM, and images revealed aggregated and irregular spherical particles [Fig. 2 (S)]. The average size of the TiO_2 NPs was ~12 nm (±1.89) and for the N–TiO_2 NPs it was ~10 nm (±1.49) [Fig. 4 (A) and 4 (B)]. Nanoparticles with FA (FA-TiO_2 and N–TiO_2-FA) exhibited average sizes of ~13 nm (±1.07) and ~12 nm (±1.91), respectively [Fig. 4 (C) and 4 (D)]. The NP size is an important factor in photocatalytic activity because smaller-sized particles have a larger surface area to interact with bacteria, meaning there is better photocatalytic action of TiO_2 on these microorganisms [49, 50].

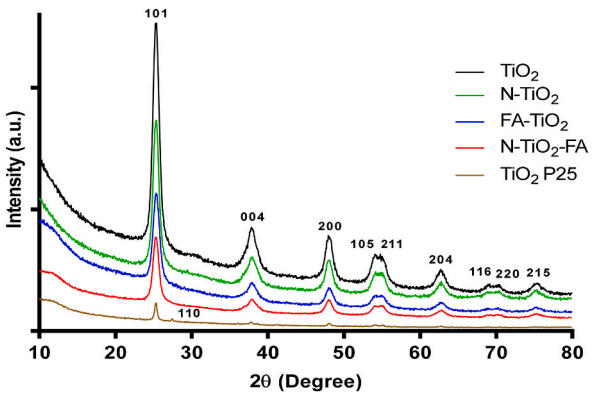

Fig. 2. X-ray diffraction characterization of TiO_2, N–TiO_2, FA-TiO_2, N–TiO_2-FA and TiO_2 P25.

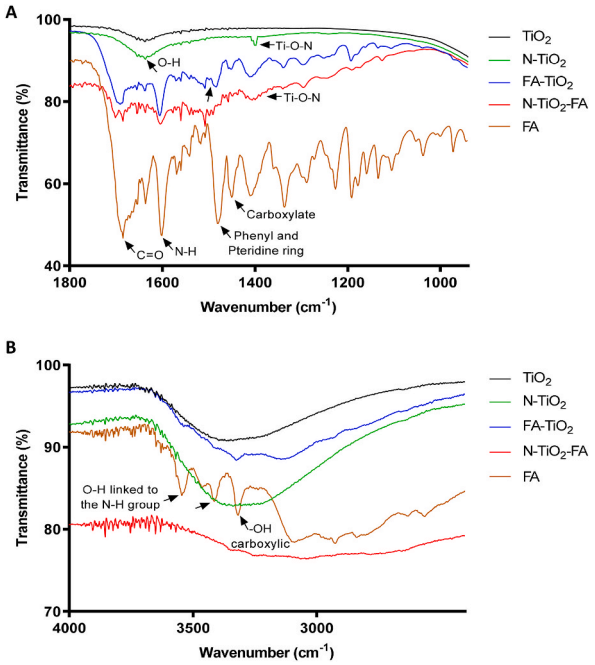

Fig. 3. Characterization by Fourier Transform Infrared Spectroscopy (FTIR) of TiO_2, N–TiO_2, FA-TiO_2, N–TiO_2-FA and FA: (**A**) Overview spectral region analyzed, (**B**) magnification between 1800 and 940 cm^{-1}.

3.2. Antibacterial photocatalytic test

The photocatalytic effect of NPs on planktonic bacteria *P. aeruginosa, S. aureus,* and MRSA was studied under dark, UV, and visible light conditions at 0, 60, 120, and 180 min [Figs. 5 (A), 6 (A), and 7 (A)].

Under UV conditions, the growth control showed that bacteria were completely inhibited [Fig. 5 (A), 6 (A), and 7 (A)]. This UV effect on resistant bacteria was also observed in previous work, attributed to the bacterial oxidative stress defense mechanism [51,52]. Next, the photocatalytic activity of N–TiO_2-FA and FA-TiO_2 under UV was observed on *P. aeruginosa* at 60 min and 180 min, respectively [Fig. 5 (A) and 5 (D)]. The same photocatalytic effect of FA-TiO_2 and N–TiO_2 was found at 180 min, and it should be noted that the effect of FA-TiO_2 on *P. aeruginosa* has not previously been demonstrated in the literature.

Concerning *S. aureus* growth under UV irradiation, N–TiO_2-FA inhibited bacterial growth at 180 min, while N–TiO_2 had the same effect at 60 min [Fig. 6 (A) and 6 (D)]. A bacteriostatic effect of TiO_2 NP at 180 min was observed, suggesting the toxicity of this nanoparticle on *S. aureus* under UV irradiation. Regarding MRSA analysis, FA-TiO_2 and N–TiO_2-FA promoted a bacteriostatic effect at 60 min and growth inhibition at 120 min, similar to N–TiO_2 [Fig. 7 (A) and 7 (D)]. Although nitrogen doping improves the photocatalytic activity of TiO_2 under visible light, it still absorbs in the UV region [53], explaining the N–TiO_2 effect under the UV condition. The bacterial growth inhibition may be due to the synergistic effect of NPs and UV, which promote chemical reactions with biological molecules (proteins, DNA, and lipids), causing cell damage [9].

Meanwhile, the photocatalytic activity of NPs with FA may be due to the tendency of microorganisms to accumulate near sources with folate [23] derived from these photocatalysts. Therefore, the bacterial affinity for these photocatalysts with FA (TiO_2-FA and N–TiO_2-FA) would lead to cell wall damage during photocatalysis. Additionally, NPs conjugated to FA absorb radiation in the UV–Vis region, evidencing its photocatalytic capacity for biological applications.

Photocatalysis under visible light and dark conditions against *P. aeruginosa* had no antimicrobial effect [Fig. 5 (B) and 5 (C)]. As expected, non-nitrogen-doped nanoparticles did not show photocatalytic activity under visible light, but there was also no observed photocatalytic capacity of nitrogen-doped nanoparticles against *P. aeruginosa*. This could be due to the Gram-negative characteristic of *P. aeruginosa*, which contains peptidoglycan between the inner membrane and outer cell membrane, thus increasing bacterial protection. In addition to the cell membrane structure, the exposure time and nanoparticle concentration may also be limiting factors in the photocatalytic activity of N–TiO_2 nanoparticles [54].

Concerning the treatment under visible light on *S. aureus*, N–TiO_2 and N–TiO_2-FA reduced the cell viability completely at 120 min and 180 min, respectively [Fig. 6 (B) and 6 (D)]. According to Ref. [55], NPs doped with N exhibit a better effect under visible light than pure TiO_2 due to their lower band gap energy value, which allows for efficient absorption of visible photons, meaning less activation energy is required for ROS production. Therefore, under visible light, N–TiO_2 and N -TiO_2 -FA can have a bactericidal effect on *S. aureus*, a Gram-positive bacterium.

Additionally, N–TiO_2 and FA-TiO_2 promoted a bactericidal effect on MRSA under visible light at 180 min [Fig. 7 (B) and 7 (D)]. The ability of N–TiO_2 NPs to inhibit the MRSA growth under visible light was also observed by Ref. [56]. However, the photocatalytic effect

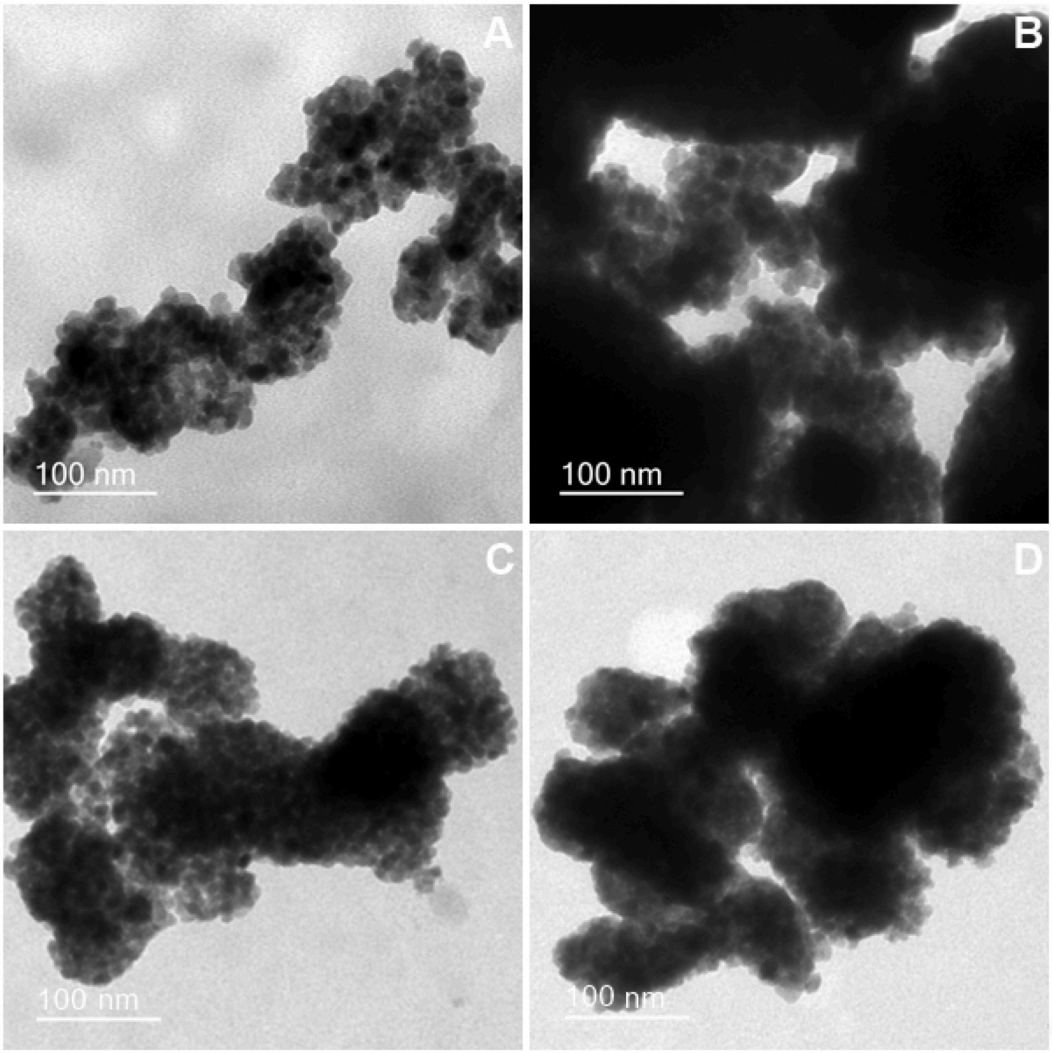

Fig. 4. Transmission Electron Microscopy (TEM) of nanoparticles (**A**) TiO_2; (**B**) N–TiO_2; (**C**) FA-TiO_2; (**D**) N–TiO_2-FA.

of TiO_2 conjugated to FA against MRSA has not previously been reported.

According to Ref. [57], FA is a nutrient necessary to synthesize nucleotides in bacteria, which may have facilitated the FA-TiO_2 entry into the cell to promote photocatalysis, leading to cell damage. Concerning N–TiO_2-FA, no bactericidal activity against MRSA under visible light was observed, which could be due to the short photocatalysis time or to the inherent resistance mechanism of efflux pumps in this bacterial strain [58,59].

Regarding the treatment under dark conditions, inherent toxicity of TiO_2, N–TiO_2, and N–TiO_2-FA was observed (bacteriostatic effect) in both *S. aureus* and MRSA [Fig. 6 (C)] and [Fig. 7 (C)].

3.3. Photocatalytic test on bacterial biofilms

The bacterial strains exhibited efficient biofilm production (Table S1); therefore, they are potentially resistant to antibiotics because the biofilm matrix prevents antibiotic diffusion and decreases its effectiveness [60].

The photocatalytic treatment against *S. aureus*, MRSA, and *P. aeruginosa* biofilms under UV, visible, and dark conditions at 180 min was analyzed [Fig. 8]. Under UV irradiation, all the photocatalysts caused a disturbance in *S. aureus* and MRSA biofilms [Fig. 8 A], whereas N–TiO_2-FA showed a greater disruption of the *P. aeruginosa* biofilm.

Under visible irradiation, no photocatalyst was effective in disrupting the *P. aeruginosa* biofilm [Fig. 8 (B)]. Meanwhile, N–TiO_2 and N–TiO_2-FA showed greater biofilm disruption in *S. aureus*, while N–TiO_2 and FA-TiO_2 exhibited a greater photocatalytic effect on the MRSA biofilm, corroborating the results in the planktonic cells [Figs. 6 (B) and Fig. 7 (B)]. This antibacterial and antibiofilm effect of TiO_2 has been reported and associated with ROS production, such as hydroxyl radicals and superoxide anions, during photocatalysis [61]. ROS exhibit a significant oxidative potential that induces wall and cell membrane damage through lipid peroxidation, leading to

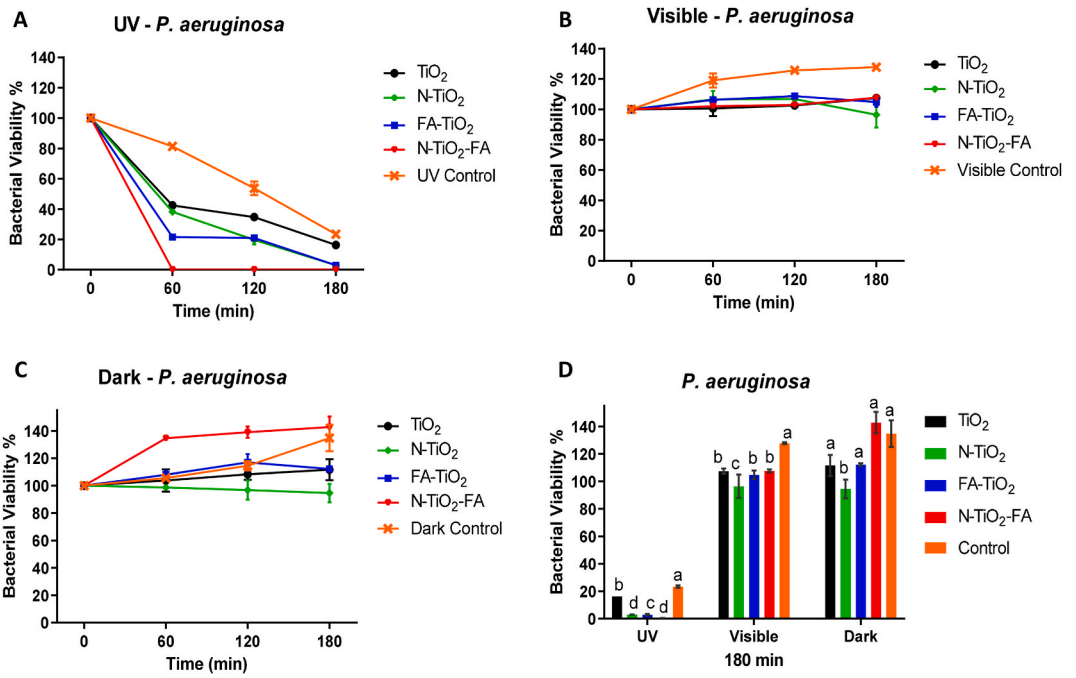

Fig. 5. Photocatalytic test at 0, 60, 120 and 180 min on *P. aeruginosa* under conditions (**A**) UV; (**B**) visible light; (**C**) dark; (**D**) photocatalysis at 180 min in the three treatment conditions. Different letters show significant differences for each treatment ($p < 0.05$).

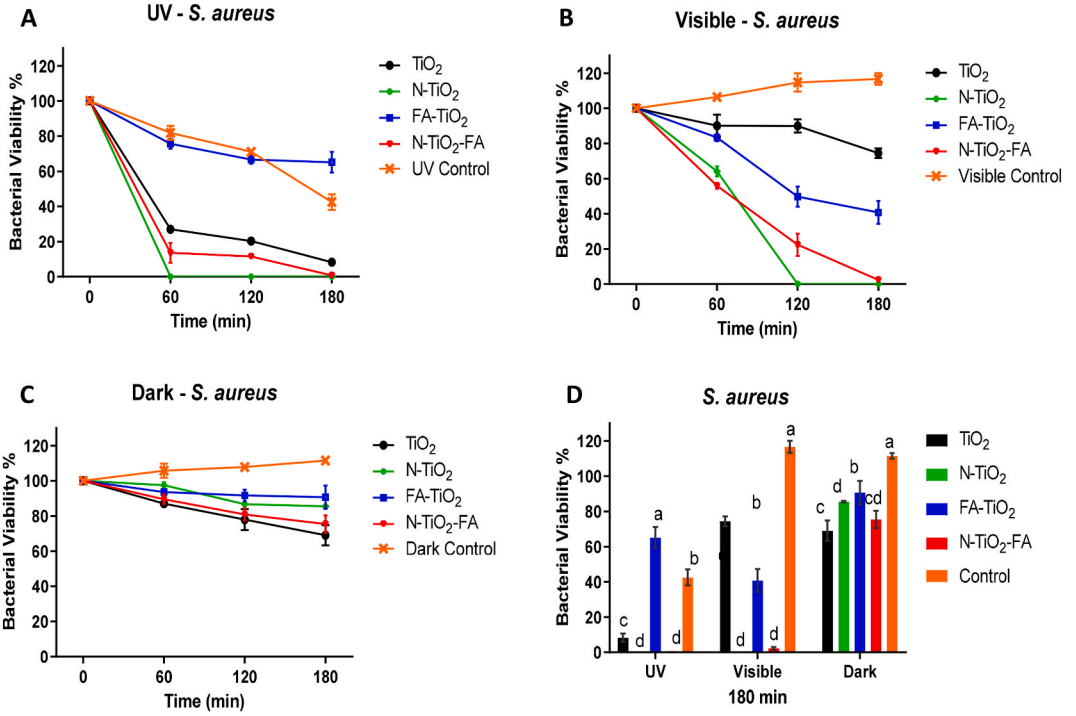

Fig. 6. Photocatalytic test at 0, 60, 120 and 180 min on *S. aureus* under conditions (**A**) UV; (**B**) visible light; (**C**) dark; (**D**) photocatalysis at 180 min in the three treatment conditions. Different letters show significant differences for each treatment ($p < 0.05$).

cell death [7,8,10,62].

Regarding the photocatalytic effect of NPs conjugated to FA, the bacteria biofilm disruption can be facilitated by greater cellular absorption of these NPs, since folate is required for cell multiplication [17]. As in planktonic cells, FA can facilitate the approach of

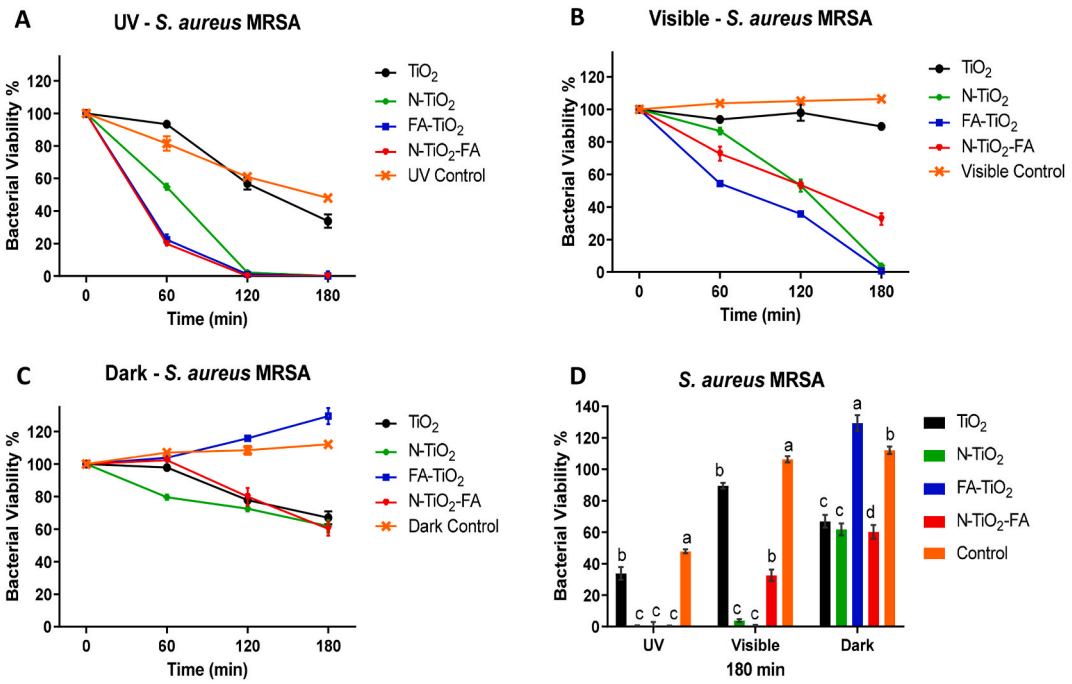

Fig. 7. Photocatalytic test at 0, 60, 120 and 180 min on methicillin-resistant *S. aureus* (MRSA) under conditions (**A**) UV; (**B**) visible light (**C**) dark; (D) photocatalysis at 180 min in the three treatment conditions. Different letters show significant differences for each treatment ($p < 0.05$).

TiO_2 to the extracellular matrix, forming ROS and leading to damage of biofilm components through oxidative stress.

The different photocatalytic effects of nanoparticles on *P. aeruginosa* and *S. aureus* biofilms can be related to structural differences in the cell walls of Gram-negative and Gram-positive bacteria. Gram-positive bacteria such as *S. aureus* have a peptidoglycan layer lining the cell membrane that can interact with free radicals during photocatalysis and inhibit the bacterial growth inside the biofilm [61,63]. In addition, genes related to antimicrobial resistance, genotypic variation, and efflux pumps may be associated with the resistance capability of these bacteria [64]. Such characteristics of resistant bacteria may explain the different effects of NPs on *S. aureus* strains and *P. aeruginosa*.

Under dark conditions [Fig. 8 (C)], the effect of nanoparticles on *P. aeruginosa* biofilm was not observed. However, TiO_2, N–TiO_2, and N–TiO_2-FA affected the biofilm integrity in *S. aureus* and MRSA under this condition, suggesting the toxicity of TiO_2 in the absence of light, which was also observed in planktonic cells.

As they had the best photocatalytic effects on MRSA and *P. aeruginosa* biofilms, nanoparticles N–TiO_2-FA (under UV irradiation) and N–TiO_2 (under visible light) were selected for analysis with AFM [Figs. 9 and 10]. The topographic analysis without photocatalytic treatment showed a homogeneous biofilm with full cells of MRSA [Fig. 9 (A) and 9 (B)]. However, in the UV treatment without photocatalysts, a disruption of the biofilm was observed with moderate changes in the shape of the cell [Fig. 9 (C) and 9 (D)]. Under visible light without photocatalysts [Fig. 9 (E) and 9 (F)], changes in cell shape were observed but no disruption to the biofilm.

In tests with the photocatalysts N–TiO_2-FA (under UV) and N–TiO_2 (under visible light), marked changes were observed in the cell surface morphology and severe disruption to the biofilm of MRSA [Fig. 9 (G) and 9 (I)] when compared with UV treatment [Fig. 9 (C)]. These changes in the MRSA cell membrane, with a cracking appearance under UV/N–TiO_2-FA treatment and under N–TiO_2/visible light treatment [Fig. 9 (H) and 9 (J)], suggest membrane destabilization, which inhibits bacterial growth and leads to cell death.

The topographic analysis of the *P. aeruginosa* biofilm and its cells was performed [Fig. 10 (A) and 10 (B)]. It was observed that UV light disrupts the biofilm (Fig. 10C) and causes changes in cell membrane morphology (Fig. 10. D). These changes were greater and more evident in the N–TiO_2-FA and UV irradiation treatment, in both biofilm and cells [Fig. 10 (E) and 10 (F)]. These changes in the biofilm morphology of *P. aeruginosa* are an important characteristic of TiO_2 NPs' interaction with the bacterial membrane, as reported by [65].

The AFM analyses showed a change in biofilm appearance of both MRSA and *P. aeruginosa* strains, as well as a decrease in cellular density at 180 min of photocatalysis, suggesting structural damage to biofilms. The major factor that inhibits bacteria and consequently their biofilm is the interaction of ROS with the bacterial membrane, inducing the denaturation of biological macromolecules such as proteins and lipids [10,62]. Therefore, the use of antimicrobial nanoparticles has been proposed due to the inefficacy of antibiotics against bacterial biofilm-linked infections [66]. Therapy failures of antibiotics against biofilms are associated with a low permeability of drugs through the biofilm matrix [1]. However, our results showed that TiO_2-FA photocatalysts have the potential to disrupt the biofilms of antibiotic-resistant bacteria.

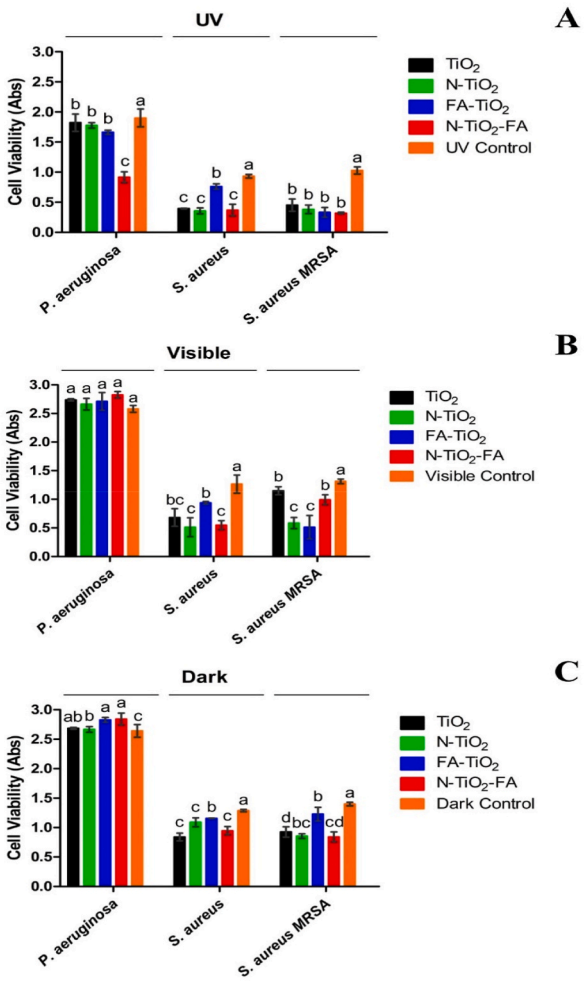

Fig. 8. Photocatalytic test on biofilms produced by *P. aeruginosa*, *S. aureus* and *S. aureus* MRSA under (**A**) UV, (**B**) visible light, and (**C**) dark conditions at 180 min. Different letters show significant differences for each treatment ($p < 0.05$).

3.4. Cell viability and CBMN assay

The toxicity of TiO_2 NPs was assessed by measuring the decrease in mitochondrial activity using the MTT assay. The cell viability was analyzed at 0.25 mg/mL, 0.5 mg/mL, and 1 mg/mL [Fig. 11 (A)]. No toxicity of the nanoparticles was observed in any treatments studied since the CHO–K1 cell exhibited viability above 70 % [Fig. 11 (A)].

Studies using TiO_2 NPs showed low toxicity in several cell lines up to 72 h of exposure [67,68]. Furthermore, conjugation of TiO_2 or other metallic NPs to folate at 1 mg/mL also has low or no toxicity in HeLa cells [10,69]. This low toxicity of folate-conjugated nanoparticles was confirmed by a cell viability above 95 % [as can be observed in Fig. 9 (A), showing that these samples are biocompatible.

In CBMN assays, we analyzed NPs at 0.25 mg/mL, 0.5 mg/mL, and 1 mg/mL [Fig. 1 (S)]. In the MN test, no differences were observed between the treatments and the negative control. The low MN frequency indicated a low rate of chromosomal breakage caused by the nanoparticles [Fig. 11 (B)]. The analysis of the frequency of NPBs and NBUDs in cells exposed to NPs [Fig. 11 (B)] also showed a low number of altered cell nuclei, indicating low cell genomic instability. Pure TiO_2 at 1 mg/mL has already been shown to have few genotoxic effects on human cells up to 24 h [65,70]. The NDI of the cells treated with NPs was not significantly different from the negative control, indicating that TiO_2 NPs have no cytostatic effect [Fig. 11 (C)]. The weak DNA damaging potential and lack of a cytostatic effect of pure TiO_2 and that conjugated to folic acid in our work indicate that these NPs are biocompatible and hold promise for applications in different technological areas.

4. Conclusion

Folic-acid-conjugated TiO_2 nanoparticles (FA-TiO_2 and N–TiO_2-FA) were successfully synthesized. TEM images showed spherical-

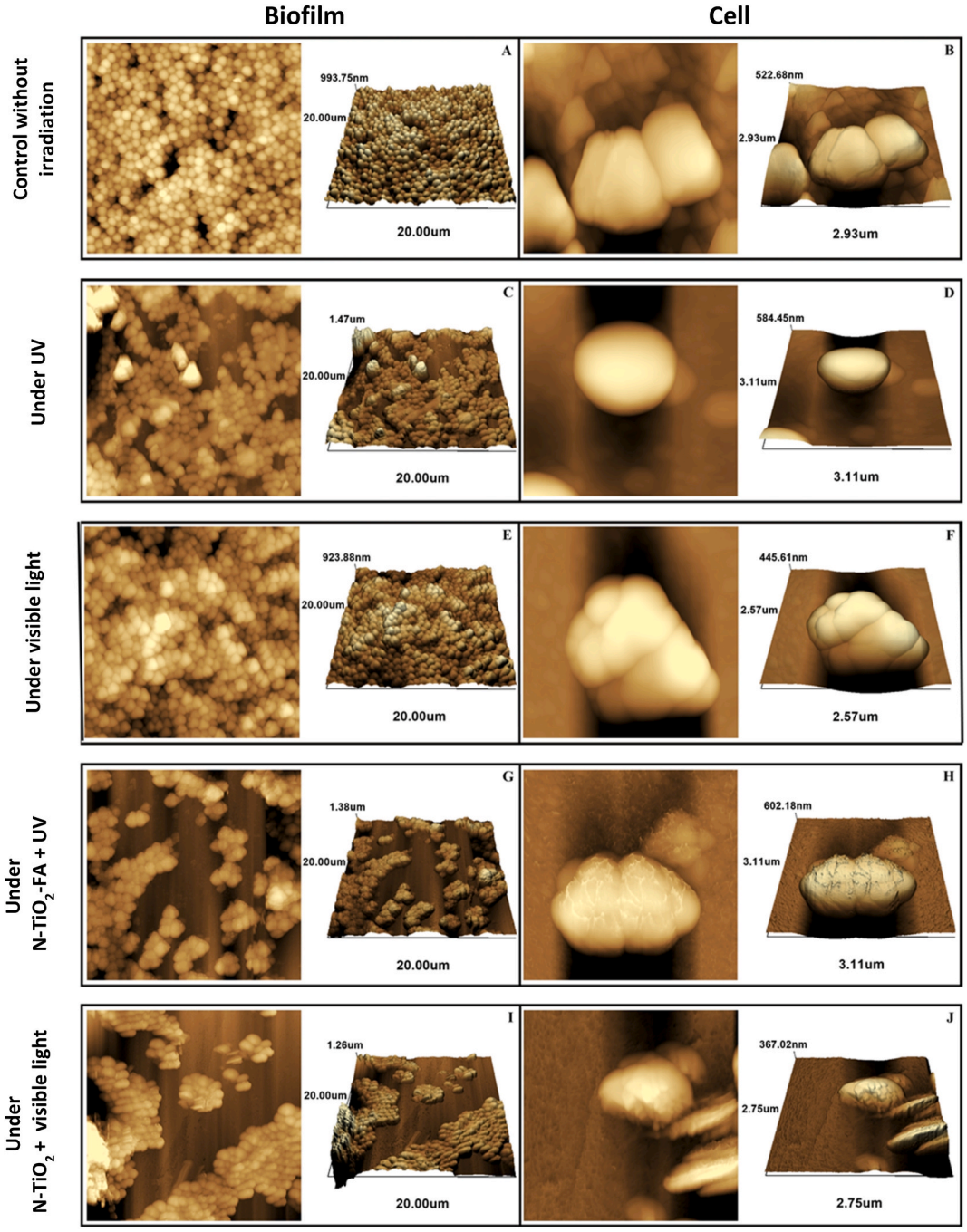

Fig. 9. Biofilm and cell structure of *S. aureus* MRSA. Control without irradiation: biofilm (**A**) and cell (**B**). Control under UV light: biofilm (**C**) and cell (**D**). Control under visible light: biofilm (**E**) and cell (**F**). Treatment under N–TiO_2-FA and UV at 180 min: biofilm (**G**), and cell (**H**). Treatment under N–TiO_2 and visible light at 180 min: biofilm (**I**) and cell (**J**).

shaped nanoparticles with sizes of 10–13 nm, and FTIR spectra demonstrated the characteristic peaks of binding between FA and TiO_2. The TiO_2 conjugated to FA demonstrated effective antibacterial activity against *P. aeruginosa*, MRSA, and *S. aureus* under UV treatment for between 60 min and 90 min. AFM images showed the rupture of biofilms formed by *P. aeruginosa* and MRSA, as well as marked changes in the bacterial membrane during photocatalysis with FA-TiO_2 and N–TiO_2-FA. No nanoparticles exhibited cytotoxic or genotoxic effects on animal cells, meaning they could be used for future technological applications. Therefore, we conclude that TiO_2-synthesized photocatalysts conjugated to folic acid are promising antimicrobial and antibiofilm agents against antibiotic-resistant bacteria and could be applied as a foundation for constructing antimicrobial materials.

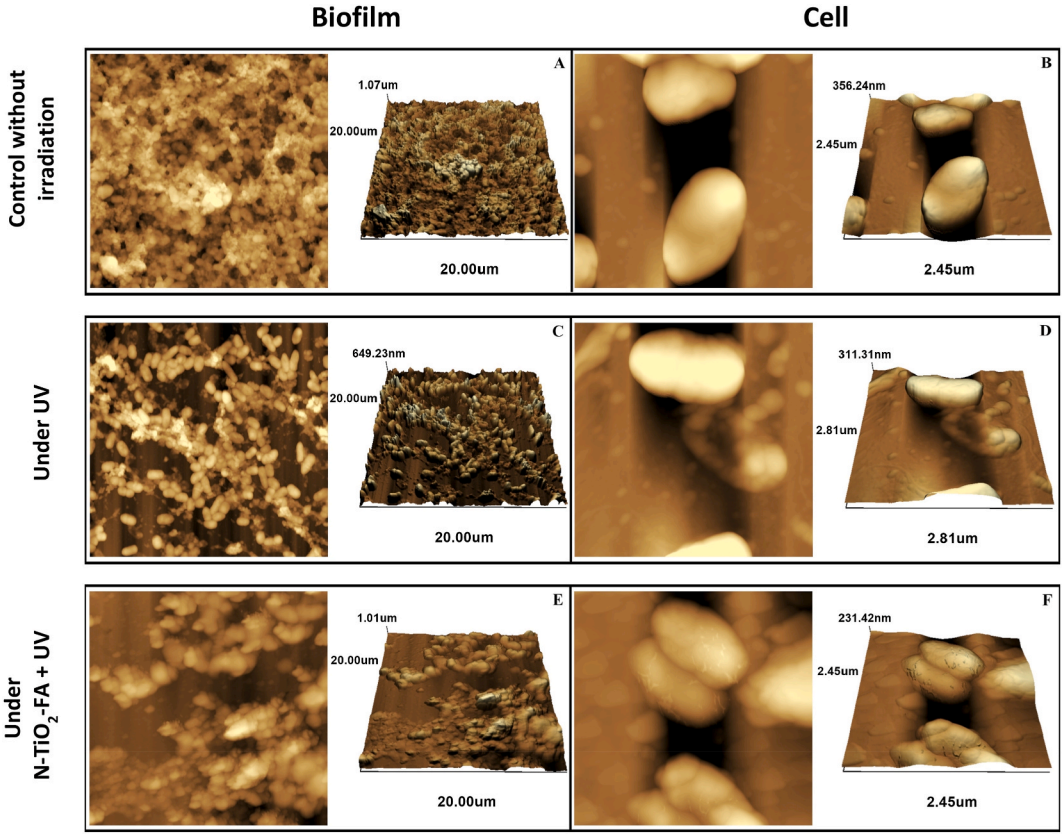

Fig. 10. Biofilm and cell structure of *P. aeruginosa* biofilm under UV photocatalysis. Control without irradiation: biofilm (**A**) and cell (**B**). Control under UV: biofilm (**C**) and cell (**D**). Treatment under N–TiO_2-FA and UV at 180 min: biofilm (**E**) and cell (**F**).

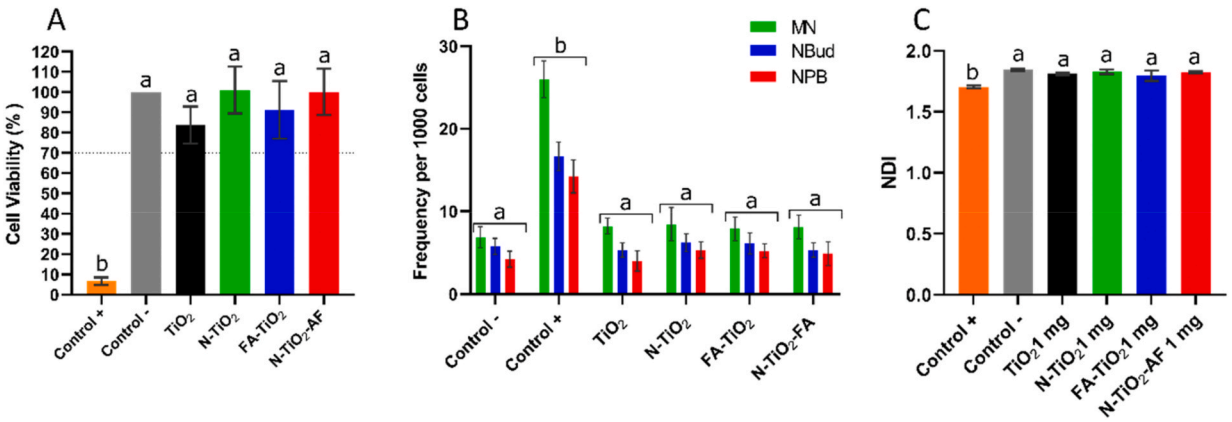

Fig. 11. Effects of the CHO–K1 cells exposure to TiO_2 NPs (1 mg/mL) on the cell viability (**A**), genotoxicity (**B**), and nuclear division index (NDI) (**C**). Frequency of micronuclei (MN), nuclear buds (NBUD), nucleoplasmic bridges (NPBs). Different letters show significant differences for each treatment ($p < 0.05$).

Funding

The authors thank the funding National Council for Scientific and Technological Development- CNPq (Grant: 01/2019-PIBIC, 305462/2021-0 DT2 and, 313662/2019-3 DT2), Coordination for the Improvement of Higher Education Personnel (CAPES) (Grant:001) and Foundation for Research and Technological Innovation Support of the State of Sergipe (FAPITEC/SE) for financial support and student fellowship.

Data availability statement

No data was used for the research described in the article.

CRediT authorship contribution statement

Raphaella I.S. Oliveira: Writing – original draft, Methodology, Investigation, Formal analysis. **Iracema N. de Oliveira:** Methodology, Formal analysis, Data curation. **Juliana F. De Conto:** Formal analysis. **Augusto M. de Souza:** Visualization, Formal analysis, Data curation. **Silvia R. Batistuzzo de Medeiros:** Validation, Formal analysis. **Silvia M. Egues:** Supervision, Funding acquisition, Formal analysis. **Francine F. Padilha:** Supervision, Formal analysis. **Maria L. Hernández-Macedo:** Writing – review & editing, Supervision, Project administration, Funding acquisition, Conceptualization.

Declaration of competing interest

The authors declare that they have no known competing financial interests or personal relationships that could have appeared to influence the work reported in this paper.

Appendix A. Supplementary data

Supplementary data to this article can be found online at https://doi.org/10.1016/j.heliyon.2023.e22108.

References

[1] K. Zhang, X. Li, C. Yu, Y. Wang, Promising therapeutic strategies against microbial biofilm challenges, Front. Cell. Infect. Microbiol. 10 (2020) 359, https://doi.org/10.3389/fcimb.2020.00359.

[2] Z. Pang, R. Raudonis, B.R. Glick, T.J. Lin, Z. Cheng, Antibiotic resistance in *Pseudomonas aeruginosa*: mechanisms and alternative therapeutic strategies, Biotechnol. Adv. 1 (2019) 177–192, https://doi.org/10.1016/j.biotechadv.2018.11.013.

[3] A.J. Haider, Z.N. Jameel, I.H. Al-Hussaini, Review on: titanium dioxide applications, Energy Proc. 157 (2019) 17–29, https://doi.org/10.1016/j.egypro.2018.11.159.

[4] X. Chen, S.S. Mao, Titanium dioxide nanomaterials: synthesis, properties, modifications, and applications, Chem. Rev. 7 (2007) 2891–2959, https://doi.org/10.1021/cr0500535.

[5] P.F. Zeni, D.P.D. Santos, R. R, J.A. Canevarolo, F.F. Yunes, R.L. Padilha, C.D. Albuquerque- Júnior, S.M. Egues, M.L. Hernández-Macedo, Photocatalytic and cytotoxic effects of nitrogen-doped TiO_2 nanoparticles on melanoma cells, J. Nanosci. Nanotechnol. 18 (2018) 3722–3728, https://doi.org/10.1166/jnn.2018.14621.

[6] T.V. Torbati, V. Javanbakht, Fabrication of TiO_2/Zn_2TiO_4/Ag nanocomposite for synergic effects of UV radiation protection and antibacterial activity in sunscreen, Colloids Surf. B Biointerfaces (2019), 110652, https://doi.org/10.1016/j.colsurfb.2019.110652.

[7] L. Zheng, S. Qian, X. Liu, Induced antibacterial capability of TiO_2 coatings in visible light via nitrogen ion implantation, Trans. Nonferrous Metals Soc. China 30 (2020) 171–180, https://doi.org/10.1016/S1003-6326(19)65189-7.

[8] B.E. Nagay, C. Dini, J.M. Cordeiro, A.P. Ricomini-Filho, E.D. Avila, R.N.C. Cruz, V.A.R. Barão, Visible-light-induced photocatalytic and antibacterial activity of TiO_2 codoped with nitrogen and bismuth: new perspective to control implant-biofilm-related disease, ACS Appl. Mater. Interfaces 11 (2019) 18186–18202, https://doi.org/10.1021/acsami.9b03311.

[9] T. Zhou, Y. Cheng, H. Zhang, G. Wang, Sunlight-mediated antibacterial activity enhancement of gold nanoclusters and graphene Co-decorated titanium dioxide nanocomposites, J. Cluster Sci. 30 (2019) 985–994, https://doi.org/10.1007/s10876-019-01558-z.

[10] X. Liang, Y. Xie, J. Wu, J. Wang, M. Petković, M. Stepić, J. Zhao, J. Ma, L. Mi, Functional titanium dioxide nanoparticle conjugated with phthalocyanine and folic acid as a promising photosensitizer for targeted photodynamic therapy in vitro and in vivo, J. Photochem. Photobiol., B 215 (2021) 1–12, https://doi.org/10.1016/j.jphotobiol.2020.112122.

[11] V.T. Nguyen, M. Tabish, G. Yasin, M. Bilal, T.H. Nguyen, C.P. Van, P. Nguyen-Tri, R.K. Gupta, T.A. Nguyen, A facile strategy for the construction of TiO_2/Ag nanohybrid-based polyethylene nanocomposite for antimicrobial applications, Nano-Struct Nano-Objects 25 (2021) 1–11, https://doi.org/10.1016/j.nanoso.2021.100671.

[12] A.A. Menazea, N.S. Awwad, Antibacterial activity of TiO2 doped ZnO composite synthesized via laser ablation route for antimicrobial application, J. Mater. Sci. Technol. 9 (2020) 9434–9441, https://doi.org/10.1016/j.jmrt.2020.05.103.

[13] S.A. Ansari, M.M. Khan, M.O. Ansari, M.H. Cho, Nitrogen-doped titanium dioxide (N-doped TiO_2) for visible light photocatalysis, New J. Chem. 40 (2016) 3000–3009, https://doi.org/10.1039/C5NJ03478G.

[14] N.A.A. Fauzi, A.J. Ireland, M. Sherriff, H.M.H.N. Bandara, B. Su, Nitrogen doped titanium dioxide as an aesthetic antimicrobial filler in dental polymers, Dent. Mater. 38 (2022) 147–157, https://doi.org/10.1016/j.dental.2021.10.019.

[15] M. Iwatsu, H. Kanetaka, T. Mokudai, T. Ogawa, M. Kawashita, K. Sasaki, Visible light-induced photocatalytic and antibacterial activity of N-doped TiO_2, J. Biomed. Mater. Res. B Appl. Biomater. 108 (2020) 451–459, https://doi.org/10.1002/jbm.b.34401.

[16] J. Ananpattarachai, Y. Boonto, P. Kajitvichyanukul, Visible light photocatalytic antibacterial activity of Ni-doped and N-doped TiO_2 on *Staphylococcus aureus* and *Escherichia coli* bacteria, Environ. Sci. Pollut. Res. 23 (2016) 4111–4119, https://doi.org/10.1007/s11356-015-4775-1.

[17] X. Chen, Y. Liu, A. Lin, N. Huang, L. Long, Y. Gang, J. Liu, Folic acid-modified mesoporous silica nanoparticles with pH-responsiveness loaded with Amp for an enhanced effect against anti-drug-resistant bacteria by overcoming efflux pump systems, Biomater. Sci. 6 (2018) 1923–1935, https://doi.org/10.1039/C8BM00262B.

[18] M. Rossi, A. Amaretti, S. Raimondi, Folate production by probiotic bacteria, Nutrients 3 (1) (2011) 118–134, https://doi.org/10.3390/nu3010118.

[19] J. Spreadbury, Folic acid and its receptors, All Capstone Projects 8 (2013). https://opus.govst.edu/capstones/8.

[20] C. Bourne, Utility of the biosynthetic folate pathway for targets in antimicrobial discovery, Antibiotics 3 (2014) 1–28, https://doi.org/10.3390/antibiotics3010001.

[21] V. de Crécy-Lagard, B. El Yacoubi, R.D. de la Garza, A. Noiriel, A. D HansonComparative genomics of bacterial and plant folate synthesis and salvage: predictions and validations, BMC Genom. 8 (2007) 1–15, https://doi.org/10.1186/1471-2164-8-245.

[22] A.R. Chowdhuri, S. Tripathy, C. Haldar, S. Chandra, B. Das, S. Roy, S.K. Sahu, Theoretical and experimental study of folic acid conjugated silver nanoparticles through electrostatic interaction for enhance antibacterial activity, RSC Adv. 5 (2015) 21515–21524, https://doi.org/10.1039/C4RA16785F.

[23] O.M. El-Borady, A.F. El-Sayed, Synthesis, morphological, spectral and thermal studies for folic acid conjugated ZnO nanoparticles: potency for multi-functional bio-nanocomposite as antimicrobial, antioxidant and photocatalytic agent, J. Mater. Sci. Technol. 9 (2020) 1905–1917, https://doi.org/10.1016/j.jmrt.2019.12.022.

[24] S. Mallakpour, M. Lormahdiabadi, Production of the ZnO-folic acid nanoparticles and poly(vinyl alcohol) nanocomposites: investigation of morphology, wettability, thermal, and antibacterial properties, J. Polym. Res. 27 (2020) 259, https://doi.org/10.1007/s10965-020-02200-7.

[25] S. Mallakpour, M. Lormahdiabadi, Polycaprolactone/ZnO-folic acid nanocomposite films: fabrication, characterization, in-vitro bioactivity, and antibacterial assessment, Mater. Chem. Phys. 263 (2021), 124378, https://doi.org/10.1016/j.matchemphys.2021.124378.

[26] J. Agnes, P. Ajith, M.M. Sappani, A.D. Prem, M.P. Soosaimanickam, J.D. Balthazar, Preparation and characterization studies of chitosan encapsulated ZnO nanoparticles modified with folic acid and their antibacterial activity against selected bacterial species, Part. Sci. Technol. (2022) 1–11, https://doi.org/10.1080/02726351.2022.2145587.

[27] Y. Xiang, X. Liu, C. Mao, X. Liu, Z. Cui, X. Yang, K.W.K. Yeung, Y. Zheng, S. Wu, Infection-prevention on Ti implants by controlled drug release from folic acid/ZnO quantum dots sealed titania nanotubes, Mater. Sci. Eng. C 85 (2018) 214–224, https://doi.org/10.1016/j.msec.2017.12.034.

[28] S. Naghibi, M. Gharagozloua, S. Vahed, Antibacterial response of Cd-TiO_2/PEG/folic acid nanocomposite under ultraviolet, visible light, or ultrasonic irradiation, J Nanostructures 9 (2019) 768–775, https://doi.org/10.22052/JNS.2019.04.018.

[29] S. Mallakpour, B. Seyfi, Antibacterial nanocomposite films based on Poly(vinyl alcohol)/TiO2-Folic acid: study of physicochemical, optical, and thermal characteristics, Mater. Chem. Phys. 281 (2022), 125809, https://doi.org/10.1016/j.matchemphys.2022.125809.

[30] D. Vilas, N. Bhanudas, G. Narendra, K. Meenal, Functionalization of AgCl/titania nanocomposite with folic acid: a promising strategy for enhancement of antimicrobial, Sci. Technol. Adv. Mater. 5 (2013), https://doi.org/10.1166/sam.2013.1472.

[31] T. Vladkova, O. Angelov, D. Stoyanova, D. Gospodinova, L. Gomes, A. Soares, F. Mergulhao, I. Ivanovac, Magnetron co-sputtered TiO_2/SiO_2/Ag nanocomposite thin coatings inhibiting bacterial adhesion and biofilm formation, Surf. Coat. Technol. 384 (2020), 125322, https://doi.org/10.1016/j.surfcoat.2019.125322.

[32] A. Sathiyaseelan, K. Saravanakumar, K.V. Naveen, K. Han, X. Zhang, M.S. Jeong, M. Wang, Combination of Paraconiothyrium brasiliense fabricated titanium dioxide nanoparticle and antibiotics enhanced antibacterial and antibiofilm properties: a toxicity evaluation, Environ. Res. 212 (2022), 113237, https://doi.org/10.1016/j.envres.2022.113237. Part B.

[33] S. Fatima, K. Ali, B. Ahmed, A.A. Al Kheraif, A. Syed, A.M. Elgorban, J. Musarrat, J. Lee, Titanium dioxide nanoparticles induce inhibitory effects against planktonic cells and biofilms of human oral cavity isolates of *Rothia mucilaginosa, georgenia* sp. and *Staphylococcus saprophyticus*, Pharmaceutics 13 (2021) 1564, https://doi.org/10.3390/pharmaceutics13101564.

[34] T.C. Jagadale, S.P. Takale, R.S. Sonawane, H.M. Joshi, S.I. Patil, B.B. Kale, S.B. Ogale, N-doped TiO_2 nanoparticle based visible light photocatalyst by modified peroxide sol-gel method, J. Phys. Chem. 112 (2008) 14595–14602, https://doi.org/10.1021/jp803567f.

[35] C. Burda, Bu, Y. Lou, X. Chen, A.C.S. Samia, Samia, J. Stout, J.L. Gole, Enhanced nitrogen doping in TiO_2 nanoparticles, Nano Lett. 3 (2003) 1049–1051, https://doi.org/10.1021/nl034332o.

[36] T. Lai, W. Lee, Killing of cancer cell line by photoexcitation of folic acid-modified titanium dioxide nanoparticles, J. Photochem. Photobiol., A: Chem 204 (2009) 148–153, https://doi.org/10.1016/j.jphotochem.2009.03.009.

[37] R.F. Iorio, M.B. Caboclo, A.G. Azevedo, F. P Barcellos, R.M. Neves, Domingues, K.R. Santos, Characteristics related to antimicrobial resistance and biofilm formation of widespread methicillin resistant Staphylococcus epidermidis ST2 and ST23 lineages in Rio de Janeiro hospitals, Brazil, Microbiol Infect Dis 72 (2012) 32–40, https://doi.org/10.1016/j.diagmicrobio.2011.09.017.

[38] S. Stepanović, D. Vukocic, I. Dakic, B. Savic, M. Svabic-Vlahovic, A modified microtiter-plate test for quantification of staphylococcal biofilm formation, J. Microbiol. Methods 40 (2000) 175–179, https://doi.org/10.1016/s0167-7012(00)00122-6.

[39] Clinical and Laboratory Standards Institute, Methods for dilution antimicrobial susceptibility tests for bacteria that grow aerobically; approved standard, in: CLSI document M07-A10, 11th ed., Clinical and Laboratory Standards Institute, Wayne, PA, 2018, p. 35. https://clsi.org/media/1928/m07ed11_sample.pdf.

[40] J.D.F. de Queiroz, A.M. de S. Leal, M. Terada, L.F. Agnez-Lima, I. Costa, N.C. de S. Pinto, S.R, Batistuzzo de Medeiros, Surface modification by argon plasma treatment improves antioxidant defense ability of CHO-k1 cells on titanium surfaces, Toxicol. Vitro 28 (2014) 381–387, https://doi.org/10.1016/j.tiv.2013.11.012.

[41] M. Fenech, Cytokinesis-block micronucleus cytome assay, Nat. Protoc. 2 (2007) 1084–1104, https://doi.org/10.1038/nprot.2007.77.

[42] M. Baibarac, I. Smaranda, A.S. Nila, Constantin, Optical properties of folic acid in phosphate buffer solutions: the influence of pH and UV irradiation on the UV-VIS absorption spectra and photoluminescence, Sci. Rep. 9 (2019), 14278, https://doi.org/10.1038/s41598-019-50721-z.

[43] D. Reyes-Coronado, G. Rodríguez-Gattorno, M.E. Espinosa-Pesqueira, C. Cab, R. Coss, G. Oskam, Phase-pure TiO_2) nanoparticles: anatase, brookite and rutile, Nanotechnology 19 (2008), 145605, https://doi.org/10.1088/0957-4484/19/14/145605.

[44] F.V. Steky, V. Suendo, R.R. Mukti, D.P. Benu, M. Reza, D.R. Adhika, V.V. Tanuwijaya, A.B. Nugraha, Bcl morphology formation strategy on nanostructured titania via alkaline hydrothermal treatment, Bull. Chem. React. Eng. Catal. 14 (2019) 513–520, https://doi.org/10.9767/bcrec.14.3.3853.513-520.

[45] W.L. Silva, M.A. Lansarin, C.C. Moro, Synthesis, characterization and photocatalytic activity of nanostructured TiO_2 catalysts doped with metals, Quím. Nova 36 (2013) 382–386, https://doi.org/10.1590/S0100-40422013000300006.

[46] Y. Liu, J. He, Y. Sun, J. Hu, C. Li, G. Xue, S. Ognier, A comparison of N-doped TiO_2 photocatalysts preparation methods and studies on their catalytic activity, J. Chem. Technol. Biotechnol. 88 (2013) 1815–1821, https://doi.org/10.1002/jctb.4029.

[47] E. Assadpour, S. Jafari, Y. Maghsoudlou, Evaluation of folic acid release from spray dried powder particles of pectin-whey protein nano-capsules, Int. J. Biol. Macromol. 95 (2017) 238–247, https://doi.org/10.1016/j.ijbiomac.2016.11.023.

[48] A. Vora, A. Riga, D. Dollimore, K. Alexander, Thermal stability of folic acid in the solid-state, J. Therm. Anal. Calorim. 75 (2004) 709–717, https://doi.org/10.1023/B:JTAN.0000027167.14746.28.

[49] X. Zhou, J. Lu, J. Jlang, X. Li, M. Lu, G. Yuan, Z. Wang, M. Zheng, H.J. Seo, Simple fabrication of N-doped mesoporous TiO_2 nanorods with the enhanced visible light photocatalytic activity, Nanoscale Res. Lett. 9 (2014) 34, https://doi.org/10.1186/1556-276X-9-34.

[50] A. Jonidi Jafari, M. Moslemzadeh, The effect of TiO_2 nanoparticles on bacterial growth: the effect of particle size and their structure - a systematic review, Int. J. Environ. Health Res. 2 (2023) 1–11, https://doi.org/10.1080/09603123.2022.2163990.

[51] M. Jiménez- Tototzintle, I.J. Ferreira, S.S. Duque, P. Rubens, G. Barrocas, E.M. Saggioro, Removal of contaminants of emerging concern (CECs) and antibiotic resistant bacteria in urban wastewater using UVA/TiO_2/H_2O_2 photocatalysis, Chemosphere 210 (2018) 449–457, https://doi.org/10.1016/j.chemosphere.2018.07.036.

[52] K.J. Clemente, A. Ramsden, F. Wright, J.A. Iza, G.L. Morrissey, D.J. Puma, Malik, Staphylococcus aureus resists UVA at low irradiance but succumbs in the presence of TiO_2 photocatalytic coatings, J. Photochem. Photobiol. B Biol. 193 (2019) 131–139, https://doi.org/10.1016/j.jphotobiol.2019.02.009.

[53] V. Etacheri, C.D. Valentin, J. Schneider, D. Bahnemann, S.C. Pillai, Visible-light activation of TiO_2 photocatalysts: advances in theory and experiments, Photochem Photobiol C: Photochem Ver 25 (2015) 1–29, https://doi.org/10.1016/j.jphotochemrev.2015.08.003.

[54] K. Gupta, R.P. Singh, A. Pandey, A. Pandey, Photocatalytic antibacterial performance of TiO_2 and Ag-doped TiO_2 against S. aureus. P. aeruginosa and E. coli, Beilstein J. Nanotechnol. 4 (2013) 345–351, https://doi.org/10.3762/bjnano.4.40.

[55] T. Makropoulou, P. Panagiotopoulou, D. Venieri, N-doped TiO_2 photocatalysts for bacterial inactivation in water, J. Chem. Technol. Biotechnol. 93 (2018) 2518–2526, https://doi.org/10.1002/jctb.5639.

[56] C.W. Dunnill, Z. Ansari, A. Kafizas, S. Perni, D.J. Morgan, M. Wilson, I.P. Parkin, Visible light photocatalysts -N-doped TiO_2 by sol–gel, enhanced with surface bound silver nanoparticle islands, J. Mater. Chem. 21 (2011) 11854–11861, https://doi.org/10.1039/C1JM11557J.

[57] C. Maynard, O. Cummins, J. Green, D. Weinkove, A bacterial route for folic acid supplementation, BMC Biol. 16 (2018) 1–10, https://doi.org/10.1186/s12915-018-0534-3.

[58] A. Vaishampayan, E. Grohmann, Antimicrobials functioning through ROS-mediated mechanisms: current insights, Microorganisms 10 (2022) 61, https://doi.org/10.3390/microorganisms10010061.
[59] S.S. Grant, D.T. Hung, Persistent bacterial infections, antibiotic tolerance, and the oxidative stress response, Virulence 4 (2013) 273–283, https://doi.org/10.4161/viru.23987.
[60] L. Sobisch, K.M. Rogowski, J. Fuchs, W. Schmieder, A. Vaishampayan, P. Oles, N. Novikova, E. Grohmann, Biofilm forming antibiotic resistant gram-positive pathogens isolated from surfaces on the international space station, Front. Microbiol. 10 (2019) 543, https://doi.org/10.3389/fmicb.2019.00543.
[61] H. Joe, Y.J. Seo, A newly designed tympanostomy stent with TiO_2 coating to reduce Pseudomonas aeruginosa biofilm formation, J Biomater Appl33 (2018) 599–605, https://doi.org/10.1177/0885328218802.
[62] M. Alavi, R. Yarani, ROS and RNS modulation: the main antimicrobial, anticancer, antidiabetic, and antineurodegenerative mechanisms of metal or metal oxide nanoparticles, Nano Micro Biosystems 2 (2023) 22–30, https://doi.org/10.22034/nmbj.2023.382133.1012.
[63] M.N. Alomary, M.A. Ansari, Proanthocyanin-capped biogenic TiO_2 nanoparticles with enhanced penetration, antibacterial and ROS mediated inhibition of bacteria proliferation and biofilm formation: a comparative approach, Cheme 18 (2021) 5817–5829, https://doi.org/10.1002/chem.202004828.
[64] X. Wang, Z. Chen, Q. Mu, X. Wu, J. Zhang, D. Mao, Y. Luo, P.J.J. Alvarez, Ionic liquid enriches the antibiotic resistome, especially efflux pump genes, before significantly affecting microbial community structure, Environ. Sci. Technol. 54 (2020) 4305–4315, https://doi.org/10.1021/acs.est.9b04116.
[65] M. Alavi, N. Karimi, Antiplanktonic, antibiofilm, antiswarming motility and antiquorum sensing activities of green synthesized Ag-TiO_2, TiO_2-Ag, Ag-Cu and Cu-Ag nanocomposites against multi-drug-resistant bacteria, Artif. Cells, Nanomed. Biotechnol. 46 (2018) 1–15, https://doi.org/10.1080/21691401.2018.1496923.
[66] A. Gupta, S. Mumtaz, C. Li, I. Hussain, V.M. Rotello, Combatting antibiotic-resistant bacteria using nanomaterials, Chem. Soc. Rev. 48 (2019) 415–427, https://doi.org/10.1039/c7cs00748e.
[67] S. Di Bucchianico, F. Cappellini, F. Le Bihanic, Y. Zhang, K. Dreij, H. L Karlsson, Genotoxicity of TiO_2 nanoparticles assessed by mini-gel comet assay and micronucleus scoring with flow cytometry, Mutagenesis 32 (2017) 127–137, https://doi.org/10.1093/mutage/gew030.
[68] S. Montalvo-Quiros, J.L. Luque-Garcia, Combination of bioanalytical approaches and quantitative proteomics for the elucidation of the toxicity mechanisms associated to TiO_2 nanoparticles exposure in human keratinocytes, Food Chem. Toxicol. 127 (2019) 197–205, https://doi.org/10.1016/j.fct.2019.03.036.
[69] A. Nahar, Kazi Hanium Maria, S.I. Liba, Md Anwaruzzaman, M.N.I. Khan, A. Islam, Shamima Choudhury, S.M. Hoque, Surface-modified $CoFe_2O_4$ nanoparticles using Folate-Chitosan for cytotoxicity Studies, hyperthermia applications and Positive/Negative contrast of MRI, J. Magn. Magn Mater. 554 (2022), 169282, https://doi.org/10.1016/j.jmmm.2022.169282.
[70] A. Zijno, I. De Angelis, B. De Berardis, C. Andreoli, M.T. Russo, D. Pietraforte, G. Scorza, P. Degan, J. Ponti, F. Rossi, F. Barone, Different mechanisms are involved in oxidative DNA damage and genotoxicity induction by ZnO and TiO_2 nanoparticles in human colon carcinoma cells, Toxicol. Vitro 29 (2015) 1503–1512, https://doi.org/10.1016/j.tiv.2015.06.009.